JTTEE5 13:432-442
DOI: 10.1361/10599630420434
1059-9630/$19.00 © ASM International

Peer Reviewed

Sintering and Creep Processes in Plasma-Sprayed Thermal Barrier Coatings

M. Ahrens, S. Lampenscherf, R. Vaßen, and D. Stöver

(Submitted May 22, 2003; in revised form June 10, 2003)

During operation at elevated temperatures, sintering processes can significantly influence the mechanical properties of thermal barrier coatings (TBCs) by increasing Young's modulus and reducing strain tolerance. These changes of the mechanical response of TBCs were investigated using free-standing plasma-sprayed TBCs in a thermomechanical analysis (TMA) facility. The time-dependent change of Young's modulus was determined in situ in a flexure mode at different annealing temperatures. In addition, relaxation processes during loading and unloading were monitored. The time-dependent deformation behavior of the TBC sample can be described by a simple viscoelastic approach (Burgers model). Viscosity data are determined as a function of annealing temperature and time.

Keywords bending tests, Burgers model, thermal barrier coatings, viscosity, Young's modulus

1. Introduction

Thermal barrier coatings (TBCs) are frequently used to increase operating temperatures and lifetime of turbine blades and vanes. A typical plasma-sprayed TBC system consists of a vacuum-plasma-sprayed MCrAlY bondcoat (BC) and an air-plasma-sprayed 7-8 wt.% yttria stabilized zirconia (YSZ) top coat. The required thermal insulation is provided by the low thermal conductivity of YSZ and further enhanced by the porous microstructure, as a result of the plasma-spray process. The BC acts as an interlock between ceramic top coat and the metallic substrate and protects the substrate from oxidation.[1-4]

A major driving force for TBC failure during thermal cycling is the coating stress caused by thermal mismatch strain, oxidation at the topcoat-BC interface, and sintering of the ceramic top coat. As was indicated earlier,[5-8] the coating stress can cause crack initiation, growth, and finally spallation of the ceramic top coat.

However, at present no reliable lifetime prediction for TBCs is available, and hence the full potential of the coatings cannot be used. To improve existing lifetime approaches,[5,9-11] a better understanding of the coating stress evolution during thermal cycling is essential. Therefore, more detailed information is required about the time and temperature dependence of the elastic response of the coating (Young's modulus),[12] as well as its ability for stress relaxation.

Literature reports various results for the Young's modulus of plasma sprayed YSZ coatings with values ranging from 5 up to 100 GPa but still considerably below the bulk value of about 200 GPa.[13-15] This broad range of values may be explained by the variable and anisotropic microstructure of the coatings, which is influenced by processing parameters and heat treatment. In addition, the measurement technique may have an impact on the results.

The elastic response of TBCs significantly depends on the direction and sign of the applied load. Different results are obtained for tensile and compressive loads as well as for loads applied parallel or normal to the lamellar coating structure. Typically, the measured value of the Young's modulus is larger under compression than under tensile load. The reason for this behavior, commonly observed at microcracked and porous plasma-sprayed coatings, is usually explained by the closure of fine pores and cracks under compression causing a stiffening, whereas tensile loads cause crack opening and hence a lower Young's modulus. This effect has been observed at uniaxially loaded specimens.[13,16]

Several techniques have been used to measure the elastic response of plasma sprayed coatings, e.g., measurement of sub-

M. Ahrens, R. Vaßen, and **D. Stöver,** Forschungszentrum Jülich GmbH, Institut für Werkstoffe und Verfahren der Energietechnik 1, D-52425 Jülich, Germany; and **S. Lampenscherf,** Siemens AG, Corporate Technology, 81730 Munich, Germany. Contact e-mail: r.vassen@fz-juelich.de.

List of Symbols

ε	strain
σ	stress
h	sample thickness
b	coating width
d	grip spacing (Fig. 2)
D	coating deflection
L	load
η_1, η_2	viscosity (Fig. 3)
K_1, K_2	spring constant (Fig. 3)
E_{tot}	total elastic modulus (Eq 6)
t	time

List of Acronyms

TBC	thermal barrier coating
TMA	thermomechanical analysis
BC	bondcoat
YSZ	yttria stabilized zirconia

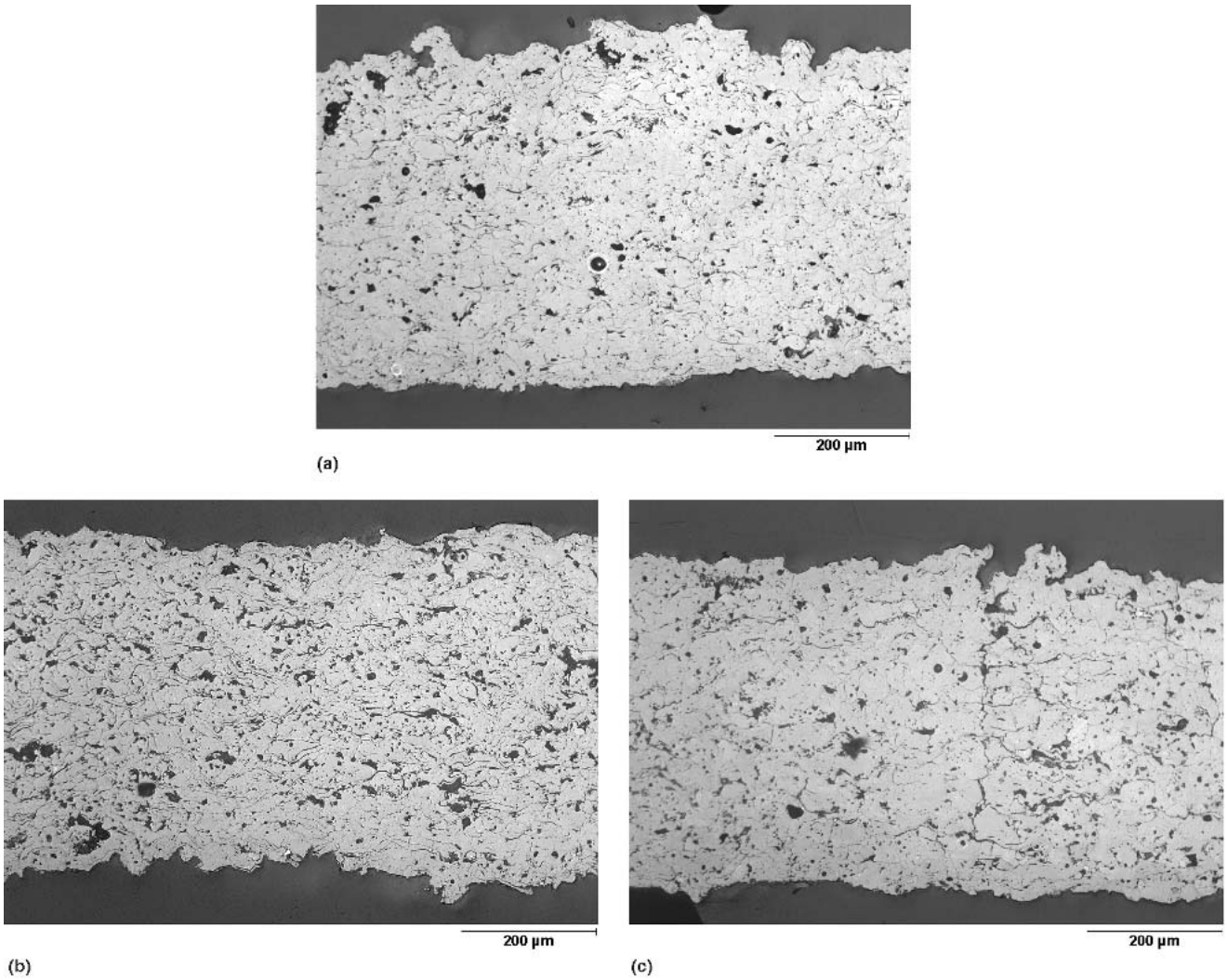

Fig. 1 Microstructures of the three types of investigated freestanding YSZ coatings: **(a)** standard-sprayed coating (porosity ~12%); **(b)** coating with higher porosity ~16%); **(c)** coating with segmentation cracks (porosity ~12%)

strate curvature caused by thermal mismatch during temperature change[17,18] and dynamic resonance measurements.[19] However, the most widely used are indentation and flexural techniques.

Using indentation techniques yields higher values of the Young's modulus approaching that of the bulk material, since the region undergoing deformation should be free from larger flaws. However, this assumption holds only for very small loads (nanoindentation). In general, a load dependence is observed.[14] Namely, the value of the Young's modulus decreases with increasing indentation load. This is a result of the increasing deformation volume more likely including pores or cracks responsible for the low values obtained with the flexural technique.

For this paper, the authors investigated the elastic response and stress relaxation of freestanding APS TBCs using a three-point bending setup. Applying extremely low loads on thin coatings in a thermomechanical analysis (TMA) device the authors investigate coatings with different microstructures at room temperature, as well as during annealing at elevated temperatures. The experimental results are interpreted using a simplified constitutive material law (Burgers Model). Finally, elasticity and viscosity data of the YSZ coatings are presented depending on the annealing stage and microstructure.

2. Experimental

The YSZ coatings were sprayed on steel substrates using an APS facility (Sulzer Metco, Wohlen, Switzerland, Triplex I gun) and Metco 204 NS powder. More details can be found in Ref 20.

Samples with three different microstructures have been obtained by changing the plasma spray conditions.

The authors investigated sintering and creep in the case of three different variations of microstructure, which are shown in Fig. 1. The variations in microstructure were achieved by changing the plasma-spray conditions. Type I specimens are sprayed under standard conditions with a porosity of about 12%. Type II specimens are coatings with higher porosity (about 16%) deposited with a reduced torch power and increased spray distance. Type III specimens are coatings with a high number of segmen-

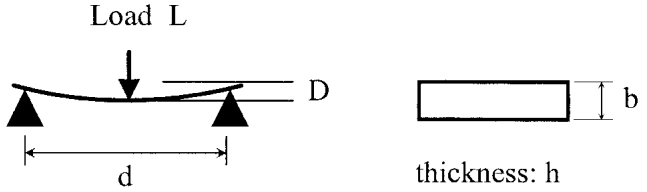

Fig. 2 Three-point bending setup used for thermomechanical analysis: Further shown is the geometry of the sample (in this particular case d = 12 mm, b = 3 mm, h = 300 μm).

tation cracks introduced by an increased amount of material deposited during one spray gun cycle. Freestanding coatings were prepared by removing the steel substrate with hydrochloric acid. Rectangular samples with a length of 15 mm and a width of 3 mm were cut from the free-standing coatings. To ensure uniform thickness of 300 μm the freestanding coatings were polished on both sides.

TMA was performed using a dilatometric device (Setsys TMA-18, SETARAM, Caluire, France) in combination with a three-point bending setup completely enclosed in a box furnace (Fig. 2). The freestanding YSZ coatings were loaded by an electromagnetically generated force (max. load 1.5 N) transduced using a wedge ended alumina rod. The coating deflection was detected by the differential transformer of the TMA head. The bending strain at sample surface can be calculated by:[21]

$$\varepsilon = \frac{6h}{d^2} \cdot D \qquad \text{(Eq 1)}$$

where D is the coating deflection, h = 300 μm is the sample thickness, and d = 12 mm is the grip spacing. Applying a load L the sample surface is subject to an in-plane stress:

$$\sigma = \frac{3d}{2bh^2} \cdot L \qquad \text{(Eq 2)}$$

where b = 3 mm is the sample width. With the given sample geometry a load of L = 1.5 N would cause an in-plane stress of about 100 MPa at the coating surface. Therefore, to avoid damage to the samples the applied loads were restricted to a maximum of L = 0.35 N.

Applying a defined load L and measuring the deflection D the corresponding sample stress σ and strain ε can be calculated. Assuming that the coatings deform in a linear elastic way, the Young's modulus could simply be calculated from the quotient σ/ε. However, the YSZ coatings show a pronounced time dependence of the deflection/strain even at ambient temperatures. Therefore, the authors always recorded the sample deflection over a certain range of time. The detailed procedure how to extract values of Young's modulus and viscosity is explained below. Measurements were done at room temperature with as-sprayed samples and samples annealed at elevated temperature for defined times. In addition, the authors monitored the response at high temperatures to investigate sintering-related stiffening of the microstructure in situ.

3. Burgers Model

A typical example of the strain history recorded in the course of one loading/unloading cycle is shown in Fig. 3. During loading, the samples show an immediate elastic response. After reaching the maximum load, the samples show a short transition time approaching a regimen of constant strain rate for fixed load. During unloading an immediate elastic response is observed again, followed by a time-dependent decrease of the sample strain (recovery), finally reaching a residual strain value. This behavior can approximately be described by the well-known Burgers model[22] schematically shown in Fig. 3. A microstructural explanation of the model is given in the discussion section.

The model consists of a spring element K_1 representing the instantaneous elastic response during loading. The dashpot element η_1 represents the familiar creep effect (sometimes called viscoplasticity). The additional spring and dashpot elements (K_2, η_2) account for the viscoelastic effect, describing the delayed transition from the instantaneous elastic response toward the constant strain rate and also the recovery of the material during unloading.

Applying the Burgers model to describe the mechanical response of the plasma sprayed coatings one gets the following differential equation for the time-dependent coating stress $\sigma(t)$ and strain $\varepsilon(t)$:

$$\sigma + \left(\frac{\eta_1}{K_1} + \frac{\eta_1}{K_2} + \frac{\eta_2}{K_2}\right) \cdot \frac{d\sigma}{dt} + \frac{\eta_1\eta_2}{K_1K_2} \cdot \frac{d^2\sigma}{dt^2} = \eta_1 \cdot \frac{d\varepsilon}{dt} + \frac{\eta_1\eta_2}{K_2} \cdot \frac{d^2\varepsilon}{dt^2} \qquad \text{(Eq 3)}$$

in which η_1 and η_2 are values of viscosity, and K_1 and K_2 are the spring constants of the viscoelastic model described in Fig. 3.

In the special case of constant load (coating stress $\sigma(t)$ = constant) the above equation simplifies to

$$\sigma = \eta_1 \cdot \frac{d\varepsilon}{dt} + \frac{\eta_1\eta_2}{K_2} \cdot \frac{d^2\varepsilon}{dt^2} \qquad \text{(Eq 4)}$$

and the corresponding time dependence of the coating strain $\varepsilon(t)$ is given by

$$\varepsilon(t) = \underbrace{\frac{\sigma}{K_1}}_{\text{elastic}} + \underbrace{\frac{\sigma}{\eta_1} \cdot t}_{\text{viscoplastic}} + \underbrace{\frac{\sigma}{K_2} \cdot \left(1 - \exp\left[-\frac{K_2}{\eta_2} \cdot t\right]\right)}_{\text{viscoelastic}} \quad (\sigma(t) = \text{const}) \qquad \text{(Eq 5)}$$

As suggested by Eq 5, the coating strain is a superposition of three contributions. The first term represents the instantaneous elastic strain of the coating. The second term describes the viscoplastic strain linearly increasing with time under constant loading conditions (creep). Defining t^* as the duration of the constant load period, the residual creep strain would be $\sigma/\eta_1 \cdot t^*$. Finally, the third term accounts for the viscoelastic behavior of the coating material. Its characteristic time dependence (relaxation time η_2/K_2) is equivalent to the homogeneous solution of Eq 4 and, therefore, describes the recovery effect of the material after unloading (σ = 0).

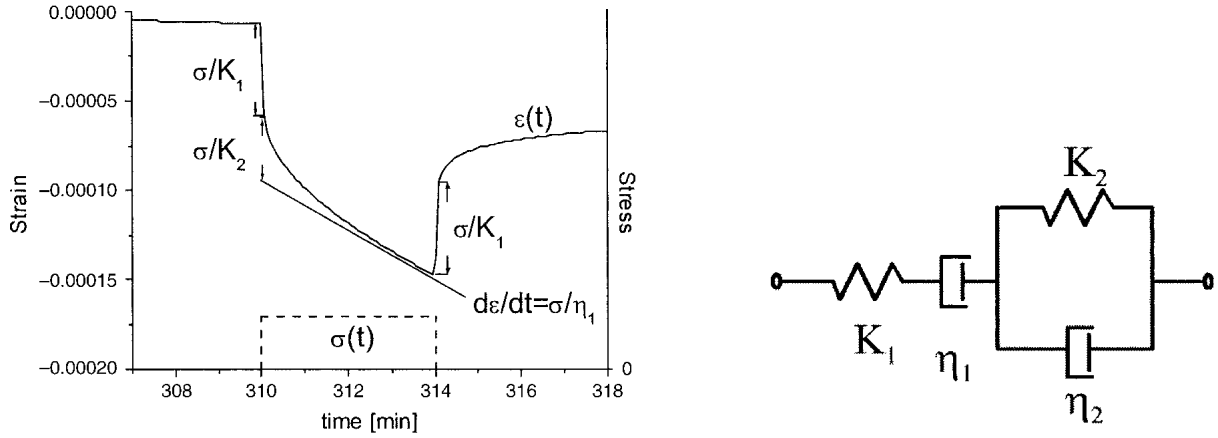

Fig. 3 Viscoelastic/viscoplastic response of in-plane strain of a specimen measured in a three-point bending setup (left); the Burgers model frequently used to describe such a behavior is shown at the right

4. Results

4.1 As-Sprayed Coatings at Room Temperature

During the first set of experiments the elastic and viscous response of the as-received coatings were investigated at room temperature.

Figure 4 shows the time-dependent strain of the as-sprayed standard coatings observed during three load cycles at room temperature. The maximum load was set to L = 0.35 N, corresponding to an in-plane stress of about 23 MPa. The creep (constant load) as well as the recovery (no load) period of the loading cycle have been set to 15 min. From Fig. 4, it can be seen that at the first loading the deflection/strain is larger compared with the following load cycles. Beginning with the second load cycle, the strain response remains almost identical (stationary) within the limits of the experimental error. Even after the sample has been removed and reinserted for a second test run, the stationary strain response is almost identically reproduced. From this observation one concludes that at the first loading cycle the sample undergoes some kind of a "plastic" strain possibly caused by a clamping effect within the porous microstructure. However, this "plastic" strain can be removed by some mechanical treatment (e.g., slight shaking), and the initial strain response of the first loading cycle shown in Fig. 4 can be reproduced. This also indicates that the coating did not crack during the bending test.

Analyzing the room-temperature tests, one focuses on the evaluation of the Young's modulus and the viscosity coefficient η_1 describing the creep behavior. According to the definition the Young's modulus is identical to the spring constant K_1 of the Burgers model (Fig. 1).

To determine K_1, one has to keep in mind that the load is not applied instantaneously but within a loading time on the order of seconds. Therefore, the transition between pure elastic and viscous strain response is blurred and an experimental error has to be taken into account for the K_1 values (about 3 MPa). Additionally, one determines the "total" elastic modulus E_{tot} describing the combined response of the two spring elements K_1 and K_2 in the Burgers model:

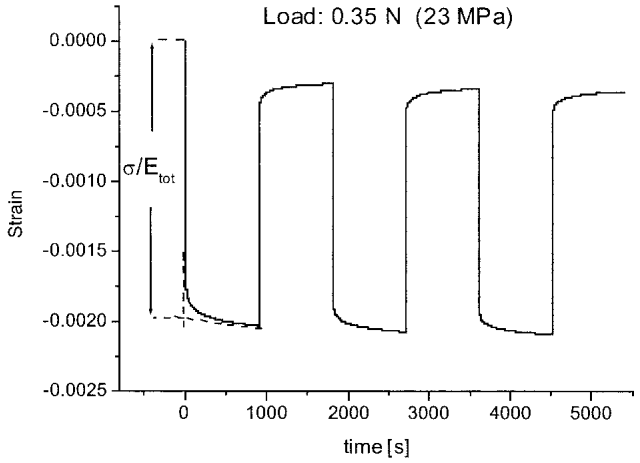

Fig. 4 Time dependence of the strain response in the case of the as-sprayed standard coating for loading the specimen three times (at room temperature)

$$\frac{1}{E_{tot}} = \frac{1}{K_1} + \frac{1}{K_2} \qquad \text{(Eq 6)}$$

Therefore, one relates the applied load to the strain that is obtained by taking the intersection of the two lines shown in Fig. 4.

The viscosity η_1 can be calculated from the strain rate $d\varepsilon/dt$ during creep (tangential slope of the strain curve) and is given by the quotient: $\sigma\, d\varepsilon/dt$. It should be mentioned that the duration of the creep phase (15 min) was not long enough to achieve an almost constant strain rate at room temperature. Therefore, the determined η_1 value should be considered as some transient viscosity value used to compare creep effects between specimens of different microstructure and heat treatment. However, the influence of this arbitrariness on the determined "total" elastic modulus E_{tot} is rather small.

The strain response measurements shown in Fig. 4 were performed at different loads. The strain taken from the intersection of the two tangent lines as well as the instantaneous elastic strain determined from the transition between pure elastic and viscous

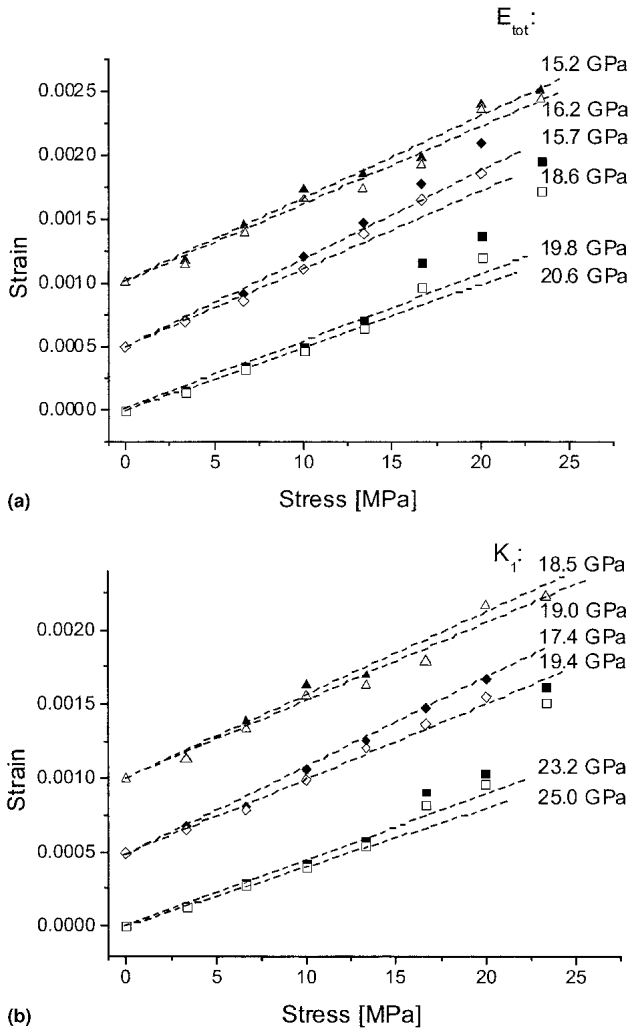

Fig. 5 Strain-stress curves for the as-sprayed coatings (at room temperature). Standard coating: squares; coating with higher porosity: diamonds; coating with segmentation cracks: triangles. **(a)** Strain related to the "total" Young's modulus E_{tot}. **(b)** Pure elastic strain, related to the "normal" Young's modulus K_1. Shown are the dependencies for the first (upper curve) and second (lower curve) loading. The results for the specimens with higher porosity and segmentation cracks are shifted along the ordinate for 0.5×10^{-3} and 1×10^{-3}, respectively.

strain response are plotted as a function of the applied in-plane stress. Results are obtained for the first and second loading cycle. For higher load, the strain-stress curves deviate from linear behavior. The values of the "total" elastic modulus E_{tot} and the Young's modulus K_1 (plotted in Fig. 5) were obtained from a linear fit of the strain-stress curves at small strains.

Figure 5 also shows the corresponding results for the as-sprayed samples coated with higher porosity and with segmentation cracks. The differences of the slope of the strain-stress curves taken from the first and second loading cycle are rather small and are within the range of the experimental error. As can be expected, the samples with standard coatings have the highest values of E_{tot} and K_1, whereas the samples with segmentation cracks or higher porosity are more compliant.

Figure 6 shows the stress dependence of the strain rate used to evaluate the viscosity of the three different types of as-sprayed

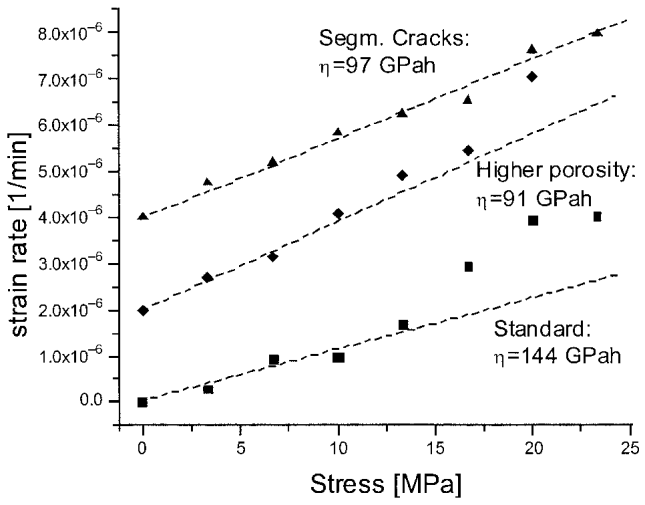

Fig. 6 Strain-rate-stress curves for the as-sprayed coatings (at room temperature). The results for the specimens with higher porosity and segmentation cracks are shifted along the ordinate for 2×10^{-6}/min and 4×10^{-6}/min, respectively.

coatings. All measurements were performed at room temperature. For clarity, the curves for the specimens with higher porosity and segmentation cracks are shifted along the ordinate.

Similar to the stiffness results, the standard coatings also show the highest viscosity value η_1. The viscosity values of the other two coating types are almost identical but 30% lower than that of the standard coating. From the significant amount of creep already observed at room temperature it is suggested that this process is caused by a sliding process between the lamellae of the YSZ coating (see discussion). Time-dependent opening of microcracks within the lamellae may additionally play a role.

4.2 Time Dependence of Elastic Modulus and Viscosity During Annealing

In the second set of experiments the evolution of the elastic and viscous response of the plasma sprayed coatings were investigated in situ during annealing.

After heating to the desired annealing temperature (heating rate: 5 *K*/min) a small load of about $L = 0.02$ N (equivalent to 1.3 MPa in-plane stress) was applied hourly for about 4 min. Figure 7 shows the complete time dependence of the strain recorded during annealing of a standard coating at 1200 °C. Every loading cycle increased the residual deformation of the flexure specimen. At the end of the measurement a total residual strain of about 0.0009 had been accumulated. Therefore, to limit the total residual strain it was necessary to keep the loads rather small. Figure 7 shows the details of two loading cycles after 4 and 28 h at 1200 °C. Comparing the measurement results with those performed at room temperature (Fig. 4) one finds a rather large strain rate at the end of the creep period that corresponds to a small viscosity value η_1 at elevated temperatures. Additionally, the instantaneous elastic response as well as the creep behavior changed during the experiment (see load cycles after 4 and 28 h in Fig. 7). In particular, the authors observed a decrease of the elastic strain and creep strain rate during annealing causing an increase of K_1 and η_1.

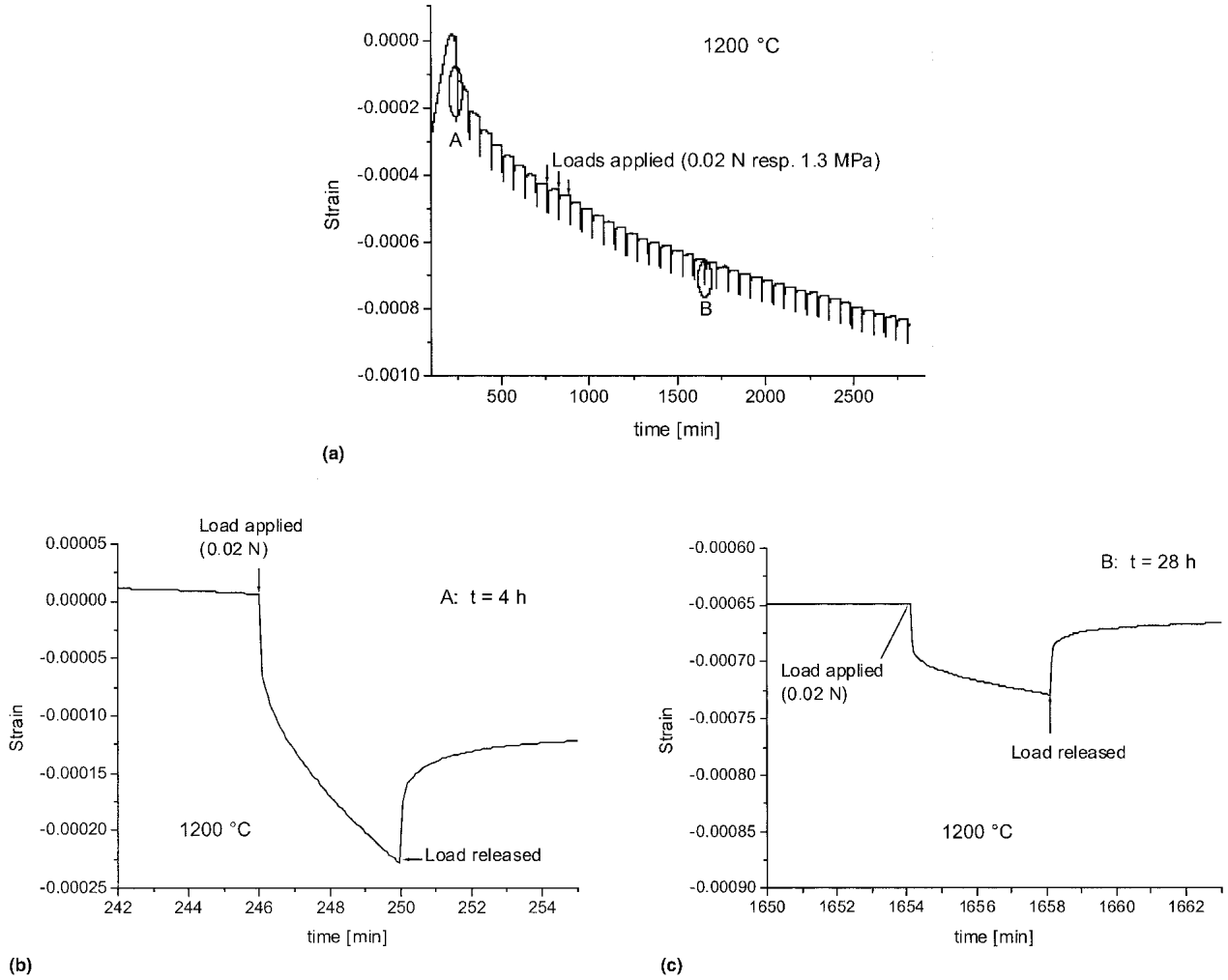

Fig. 7 Time dependence of the strain during annealing of the standard coating at 1200 °C. **(a)** A load of 0.02 N (1.3 MPa in-plane stress) was applied every hour for a duration of 4 min. In detail shown are the loading responses recorded at the times **(b)** $t = 4$ h and **(c)** $t = 28$ h.

The evolution of the elastic response and the viscous behavior during annealing was determined by evaluating the "total" elastic modulus E_{tot} and the viscosity value η_1 for each load cycle. Although the creep period (constant loading) was quite short (4 min), the strain rate reached an almost constant value at the end of this period. This has been confirmed by analyzing the time dependence of the strain rate in detail.

Figure 8 shows the results for the elastic modulus. Figure 8(a) displays the time dependence of E_{tot} at 1200 °C for different coating types, whereas Figure 8(b) shows the time dependence of E_{tot} at different annealing temperatures for the standard coatings.

Figure 9 shows the results for the viscosity η_1. Figure 9(a) displays the time dependence of η_1 at 1200 °C for different coating types, whereas Fig. 9(b) shows the time dependence of η_1 at different annealing temperatures for the standard coatings.

Elastic modulus, as well as viscosity, shows a rapid increase within the first hundred minutes of annealing. The standard coatings always show the highest final value, whereas the coatings with higher porosity or segmentation cracks are almost identical but have lower elastic modulus and viscosity values compared with the standard coatings. Furthermore, the results show that the elastic modulus and viscosity decrease with increasing temperature. Between 1000 and 1400 °C, the viscosity drops by almost two orders of magnitude.

When analyzing the strain response, one should keep in mind that sintering is activated already during heating to the annealing temperature (rate: 5 K/min). That makes it difficult to distinguish the elastic and the viscous contribution to the overall strain. The observed decrease of the elastic modulus and the viscosity at elevated temperatures may be explained by softening and sinter shrinkage of the porous coating material. At lower annealing temperatures of about 1000 °C, the authors found that ramping the sample up and down with no dwell time caused almost no change in the elastic modulus measured at room temperature. Therefore, they assume that the initial drop of the elastic modulus already observed at 1000 °C is primarily due to softening. In contrast, ramping the samples up and down to higher temperatures (1200 and 1400 °C) with no dwell time causes a change of the room-temperature value of the elastic modulus.

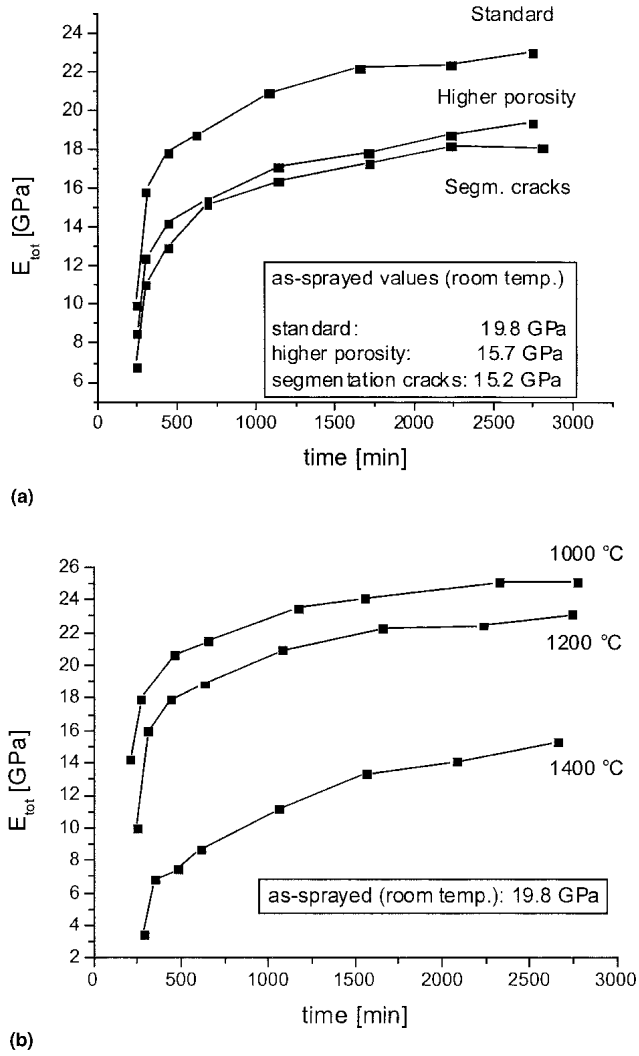

Fig. 8 Time dependence of the total elastic modulus E_{tot} during annealing at 1200 °C for **(a)** the three types of coatings and **(b)** for different annealing temperatures in the case of the standard coating; the insets show the corresponding as-sprayed values taken at room temperature.

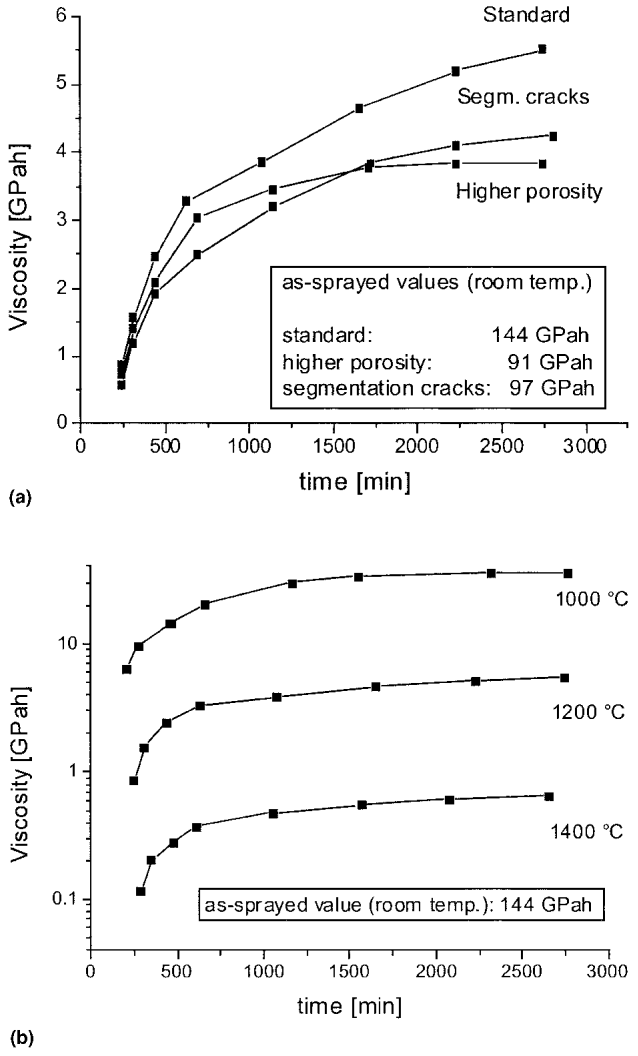

Fig. 9 Time dependence of the viscosity η_1 during annealing at 1200 °C for **(a)** the three types of coatings and **(b)** for different annealing temperatures in the case of the standard coating; the insets show the corresponding as-sprayed values taken at room temperature.

4.3 Annealed Coatings at Room Temperature

In addition to the in situ measurements, annealed coatings were tested at room temperature using the same testing procedure as that explained in Section 4.1.

The elastic and viscous response of the coatings were determined after several annealing times, not exceeding 100 h. Figure 10 shows the stress dependence of the strain and the strain rate obtained for the different types of coatings after annealing for about 100 h at 1200 °C. In the case of the standard coatings, the instantaneous elastic strain (related to the Young's modulus K_1) as well as the total strain (related to the "total" elastic modulus E_{tot}) are plotted for the first and second loading cycle. As can be seen from Fig. 10, the data points of first and second loading cycle almost coincide and the difference between E_{tot} and K_1 is lower than 1.5 GPa. This behavior was also found for coatings with higher porosity or segmentation cracks, and, therefore, only the stress dependence of the "total" strain and the value of E_{tot} is shown for these specimens.

In contrast to the room-temperature measurements of the as-sprayed coatings, the annealed samples of all coating types showed an almost linear stress-strain dependence throughout the whole range of the applied loads. According to the results of the in situ measurements, the room-temperature measurements also show the increase of the "total" elastic modulus E_{tot} and the viscosity η_1 with increasing annealing time. Figure 11 presents the evolution of the room-temperature values of the "total" elastic modulus E_{tot} and viscosity η_1 depending on annealing time at 1200 °C. For short annealing times, a rapid increase of E_{tot} and η_1 is observed. This is in accordance with the results of the in situ measurements (Fig. 8 and 9). Furthermore, the room-temperature measurements of the annealed standard coatings also indicate the highest E_{tot} values compared with the other coatings and show a monotonous increase of E_{tot} with increasing annealing time. However, in contrast to the results of the in situ experiments the room-temperature measurements of the annealed coatings with segmentation cracks exhibit a de-

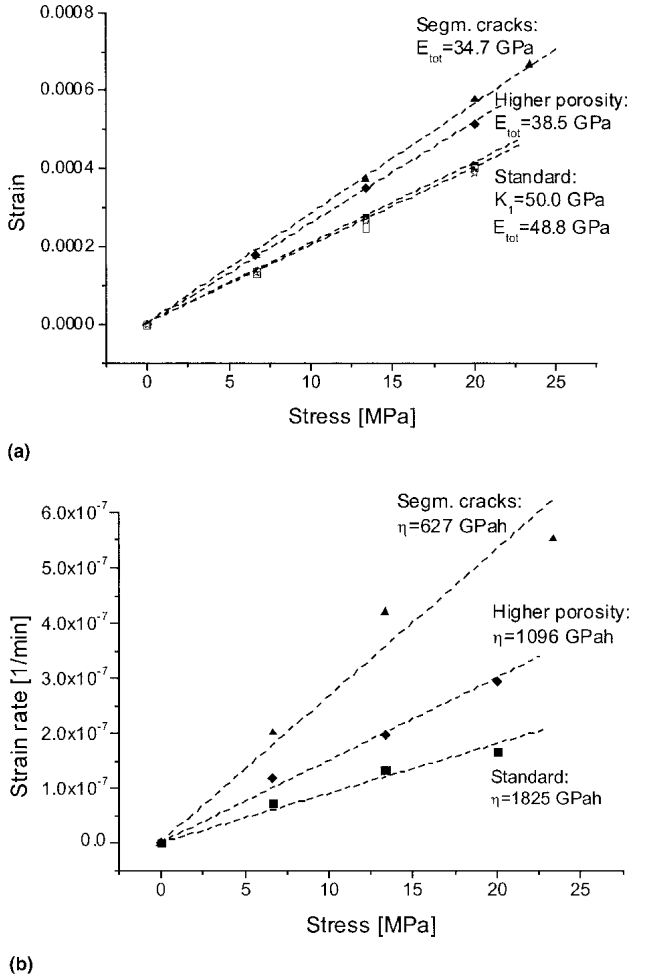

Fig. 10 **(a)** Strain-stress and **(b)** strain-rate-stress curves for coatings annealed for 100 h at 1200 °C (taken at room temperature)

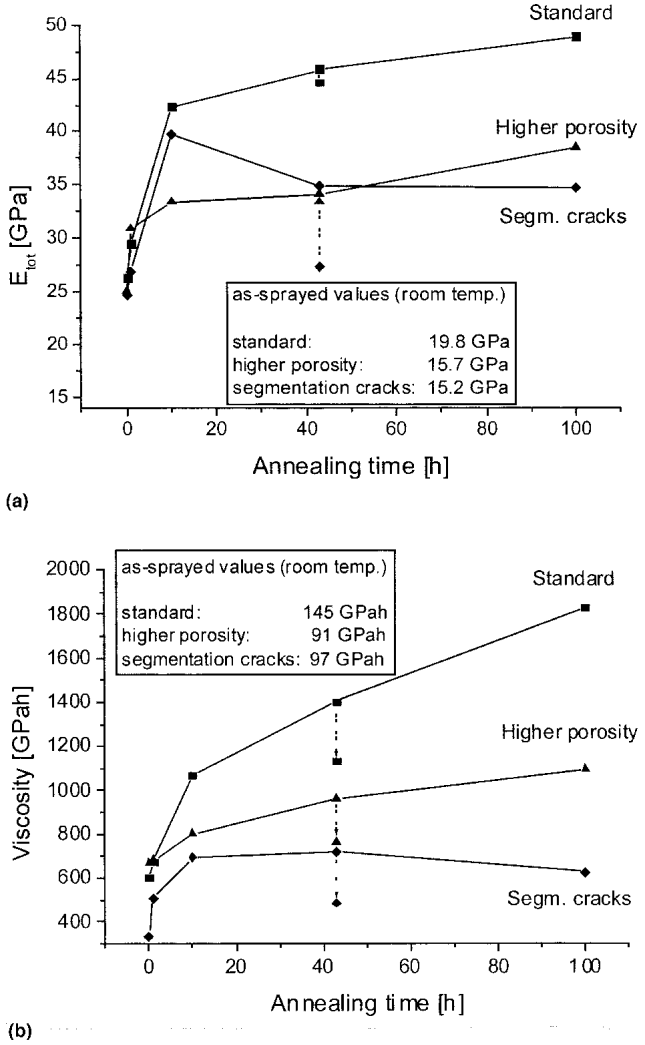

Fig. 11 Dependence of the **(a)** total elastic modulus E_{tot} and **(b)** viscosity (measured at room temperature) on annealing time at 1200 °C. Additional lower data points at 43 h annealing time are explained in the text.

crease of the "total" elastic modulus for annealing times longer than 10 h.

Figure 11 also shows the room-temperature values of E_{tot} for the coatings that were used for the in situ experiments (additional cyclic mechanical load during annealing). The total accumulated annealing time of these samples was about 43 h. As can be seen from Fig. 11, the E_{tot} as well as the viscosity values η_1 of these samples are lower than for coatings with no additional mechanical load. The "total" elastic modulus of the segmented coatings seems to be more sensible for additional mechanical load, whereas the viscosity values η_1 behave similarly for all types of coatings.

Table 1 summarizes the values of E_{tot}, K_1, K_2, and η_1 for the as-sprayed condition and after 100 h heat treatment at 1200 °C. At this point, it should be mentioned again that the room-temperature values η_1 represent a transient value of the viscosity taken after 15 min of loading. Using Eq 6, K_2 was calculated from E_{tot} and K_1. In general, K_2 seems to have larger values than K_1 (Young's modulus) with a significant increase after annealing. It was not possible to extract values for the viscosity η_2 (second dashpot element of the Burgers model). Using Eq 5, the authors tried to fit the model solution for $\varepsilon(t)$ to the measured transition region between instantaneous elastic and viscous response. However, the fit did not give satisfying results for the material parameters. This problem indicates that the Burgers model may be too rough and needs to be extended. A first improvement of the Burgers model could be to modify the stress dependence of the strain rate by introducing additional dashpots and springs in the viscoelastic element of the Burgers model or by extending the model toward a nonlinear behavior. This would introduce additional material parameters to be fitted with experiment or cause a much higher sensitivity of the strain rate with respect to the stress.

5. Discussion

The mechanical loading of the TBC samples under three-point bending is discussed first.

In three-point bending, the plasma-sprayed coatings are loaded by an overall in-plane stress distribution, where the term

Table 1 Elastic Moduli E_{tot}, K_1 and K_2 and Viscosity of As-Sprayed and Annealed Coatings Measured at Room Temperature (Annealing was 100 h at 1200 °C)

	Standard, As-Sprayed	Standard, 100 h	Higher Porosity, As-Sprayed	Higher Porosity, 100 h	Segmentation Cracks, As-Sprayed	Segmentation Cracks, 100 h
E_{tot}, GPa	19.8	48.8	15.7	37.8	15.2	34.7
K_1, GPa	23.2	49.9	17.4	39.1	18.5	36.0
K_2, GPa	135.1	2213.7	160.7	1136.9	85.2	960.9
η_1, GPah	144	1825	91	1132	97	755

overall indicates an averaged quantity (e.g., by using a representative volume element of the heterogeneous microstructure). The maximum compressive/tensile stress is found on the surface of the coating at the location of the central grip. Assuming homogeneous and linear elastic coating material, Eq 2 can be used to evaluate the maximum compressive/tensile stress at the surface of the coating. In this case, the neutral axis is in the middle of the flexure beam. However, the results of previous investigations suggest that the elastic response of freestanding TBCs is different under compressive and tensile load[13] and, therefore, nonlinear. Typically, the Young's modulus is found to be smaller under tension than it is under compressive load. Accordingly, the neutral axis is shifted toward the compression side during bending. In the limiting case of a very high Young's modulus under compression compared with its value under tension, the linear-elastic analysis of the bending test would overestimate the "tensile" Young's modulus by a factor of four. As an example, in Ref 13, the elastic behavior of freestanding plasma-sprayed TBCs was separately investigated under compression and under tension. The values obtained at room temperature were reported to be about 14 GPa under tension and about 27 GPa under compression. Taking these values the neutral axis in bending would be shifted toward the compression side by about 0.2 of the sample thickness. Unfortunately, for the analysis of our tests, the authors did not have sufficient information about the asymmetric behavior of the coatings with respect to tensile or compressive load. As an approximation, they assume linear-elastic material behavior, and consequently, the reported values of E_{tot}, K_1, and K_2 are over- or underestimated with respect to tensile or compressive load, respectively. Nevertheless, the reported values are suitable to characterize coatings with different microstructures and can be used to compare the evolution of their elastic properties during annealing.

Before discussing the results of the bending tests, a microscopic interpretation of the Burgers model is given.

As was already mentioned, the first spring element K_1 describes the instantaneous elastic response of the inhomogeneous coating microstructure when an external load is applied. The determined values of K_1 are considerably smaller than the bulk value of zirconia (200 GPa). This observation could be related to the porosity of the plasma-sprayed coatings reducing the Young's modulus. However, the porosity of the coatings discussed in this article is too small to explain the very low values of the Young's modulus measured via bending. Assuming about 15% porosity and the pore volume to be surrounded by a zirconia matrix, the effective field approximation[23] would predict an effective value of the coatings Young's modulus of the coatings of about 150 GPa. Even allowing open porosity (no matrix phase) would not drastically reduce the effective value of the Young's modulus of the coatings (effective medium approximation).

An explanation of this discrepancy may be the presence of inter- and intrasplat microcracks separating and segmenting the spray splats, respectively. The intersplat microcracks may enable a relative motion and bending of the splats, whereas the intrasplat microcracks reduce the stiffness of the splats itself. It is assumed that these two species of microcracks are responsible for the apparent low values of the Young's modulus of the coatings.

The observation of an increasing strain at constant load (creep) may be explained by the relative sliding of the splats. This sliding motion is limited by the action of friction forces caused by the rough interface of the spray splats and their nonplanar geometry. This behavior is described by the first friction element η_1. At high temperatures, diffusion processes can assist the sliding mechanism and, therefore, reduce η_1 (i.e., following the Arrhenius law).

The microscopic interpretation of the second spring and dashpot elements is more difficult. A possible explanation is to assume that the relative sliding motion of the individual spray splats does not start simultaneously. This may be due to an inhomogeneous load distribution and varying friction forces between the splats causing a transition time for the onset of the overall creep motion.

At the beginning of the loading, almost all splats carry the load, i.e., the instantaneous elastic response (Young's modulus) is high. However, over the course of time, more and more splats start to slide until a stationary motion is established. The characteristic transition between the instantaneous elastic response and the stationary creep motion is described by the ratio η_2/K_2 of the values of the second dashpont and spring element. During the stationary creep the number of load-bearing splats ("elastic backbone") of the coating is reduced, causing a lower value of the "total" elastic modulus (E_{tot}). During unloading, the creep motion stops, and an elastic strain is observed almost identical to the instantaneous elastic deformation. However, the splats that carried the load during creep are still subject to a residual stress. After some time, this residual stress is released in a reversed creep process (recovery) characterized by the same transition time η_2/K_2.

The following paragraphs discuss the results of the bending experiments, especially the effect of heat treatment on the material parameters.

The observed increase of the Young's modulus during heat treatment of the coatings is known from literature and usually explained by the activation of sintering processes.[14,24] Sintering has been observed to effectively increase the intersplat contact area (formation of sinter necks) and to heal the intrasplat microcracks.[25] Both processes effectively increase the coating

stiffness during annealing, although the amount of increase and the activation energies may be different. It is interesting to note that during heat treatment of the samples the parameter K_2 increased much more than K_1. This observation can be understood according to the authors' microscopic interpretation of the Burgers model. Even without heat treatment, almost all splats contribute to the instantaneous elastic response of the coating (K_1). However, during stationary creep the elastic response (K_2) is effectively increased by increasing the number of load-bearing splats (formation of sintering necks). Therefore, the values of K_2 and E_{tot} are much more sensitive to heat treatment than K_1 is.

The effect of increased porosity and the presence of macroscopic segmentation cracks (running through several layers of the coating) was investigated by testing three types of coatings (as described in Section 2). As expected, the standard coatings showed the highest value of the elastic modulus in as-sprayed condition (see Table 1). The effect of porosity on stiffness is widely reported in literature. In general, a rather monotonous decrease of the elastic modulus is found with increasing porosity level.[26,27] The values of the coatings with macroscopic segmentation cracks are quite close to those found for coatings with a higher porosity level (about 16%). This effect can be explained by an effective decrease of the coating stiffness due to the presence of macroscopic segmentation cracks. However, in contrast to the coating porosity the presence of segmentation cracks may cause a more pronounced asymmetry between tensile and compressive loading.

During annealing all coatings seem to approach a saturation value of the "total" elastic modulus E_{tot} within the observation time (Fig. 8). Again, the standard coatings reach the highest value, whereas the coatings with higher porosity and macroscopic segmentation cracks behave quite similarly during the whole annealing process. However, dilatometry data show that the sintering shrinkage during annealing is substantially larger for the coatings with higher porosity than for the segmented coatings under equivalent annealing conditions.[25,28] This indicates that there is no simple correlation between volumetric shrinkage and stiffness increase during sintering. As already mentioned, the stiffness increase could be related to healing of microcracks within the spray splats (intrasplat cracks) as well as to the formation of sintering contacts between the splats (intersplat cracks). Both crack closure effects are dominated by surface diffusion and do not require substantial volumetric change of the samples. Finally, the experimental results indicate that the evolution of the effective elastic modulus of plasma-sprayed YSZ coatings is not only dictated by the evolution of total porosity, but also depends on additional microstructural details.[29]

It should also be mentioned that in the segmented coatings the growth of delamination cracks was observed after annealing. This additional defect mechanism might explain the modulus decrease of the segmented coatings observed after long-term annealing at 1200 °C (Fig. 11).

Figure 11 also shows the effect of a cyclic mechanical load during heat treatment. The samples with additional mechanical load during annealing show a reduced Young's modulus. This can be explained by a repeated breaking of sintering contacts during loading, thereby limiting the effect of stiffness increase during heat treatment.

As mentioned above, creep of the coatings is correlated to the sliding motion of the spray splats. This sliding motion is limited by the action of friction forces caused by the rough interface of the spray splats and their nonplanar geometry. The experiments suggest that this process may also happen at room temperature. At high temperatures, diffusion processes can assist the sliding mechanism. As a result, the creep rates increase with temperature and the viscosity decreases.

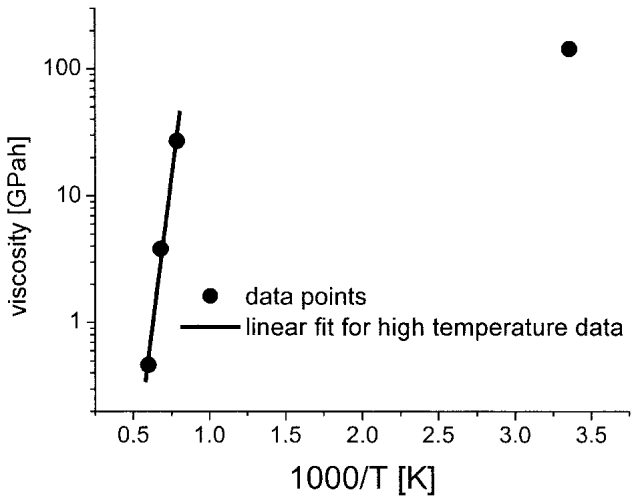

Fig. 12 Viscosity data taken from Fig. 9 at 1000 min as a function of the inverse temperature

Figure 12 shows the measured viscosity data η_1 after 1000 min annealing (compare with Fig. 9) on a logarithmic scale as a function of inverse temperature. In this Arrhenius-type plot, the high-temperature data show a linear behavior. From the slope of a linear fit the authors determined the activation energy to be 1.85 ± 0.18 eV. This value appears to be low compared with activation energies of volume diffusion (6.4 eV) and grain-boundary diffusion (5.3 eV) in YSZ.[30] An explanation might be the enhanced diffusivity at the interfaces due to impurity phases.

The influence of the annealing treatment on the viscosity can also be explained using the above model of sliding spray splats. The formation of sintering necks between the spray splats increases the threshold load for the onset of splat sliding and therefore increases viscosity with increasing annealing time. Similar to the discussion for the elastic behavior, the model also explains the viscosity reduction for the samples subject to a cyclic load during annealing (Fig. 11). Again the repeated breaking of the sintering necks promotes the sliding process in these samples and reduces viscosity.

6. Conclusions

The mechanical response of different types of plasma-sprayed thermal barrier coatings has been investigated under three-point bending at room temperature and during annealing at elevated temperature. The mechanical behavior of the coatings is described by the Burgers model and discussed on the basis of a simple microstructural interpretation.

Heat treatment of the coatings significantly increased the Young's modulus of the coating. After annealing for 100 h at 1200 °C, an increase by a factor of more than two was observed.

Simultaneously, the viscosity increased also by a factor of two. Measurements at elevated temperatures allowed the determination of the temperature dependence of the Young's modulus and the viscosity. High-temperature measurements suggest an Arrhenius type of behavior for the viscosity data, indicating a thermally activated process with rather low activation energy of about 1.9 eV.

References

1. R.A. Miller: "Current Status of Thermal Barrier Coatings–An Overview," *Surf. Coat. Technol.,* 1987, *30,* pp. 1-11.
2. J. Thornton: "Thermal Barrier Coatings," *Mater. Forum,* 1998, *22,* pp. 159-81.
3. D. Stöver and C. Funke: "Directions of the Development of Thermal Barrier Coatings in Energy Applications," *Mater. Proc. Technol.,* 1999, *92-93,* pp. 195-202.
4. R. Vaßen and D. Stöver: "Conventional and New Materials for Thermal Barrier Coatings," in *Functional Gradient Materials and Surface Layers Prepared by Fine Particles Technology,* M.-I. Baraton and I. Uvarova, ed., Kluwer Academic Publishers, Dordrecht, The Netherlands, 2001, pp. 199-216.
5. R. Vaßen, G. Kerkhoff, and D. Stöver: "Development a Micromechanical Life Prediction Model for Plasma Sprayed Thermal Barrier Coatings," *Mater. Sci. Eng. A,* 2001, *303,* pp. 100-09.
6. A. Rabiei and A.G. Evans: "Failure Mechanisms Associated With the Thermally Grown Oxide in Plasma-Sprayed Thermal Barrier Coatings," *Acta Mater.,* 2000, *48,* pp. 3963-76.
7. A.G. Evans, M.Y. He, and J.W. Hutchinson: "Mechanics-Based Scaling Laws for the Durability of Thermal Barrier Coatings," *Prog. Mater. Sci.,* 2001, *46,* pp. 249-71.
8. A.G. Evans, D.R. Mumm, J.W. Hutchinson, G.H. Meier, and F.S. Pettit: "Mechanisms Controlling the Durability of Thermal Barrier Coatings," *Prog. Mater. Sci.,* 2001, *46,* pp. 505-53.
9. M.-J. Pindera, J. Aboudi, and S.M. Arnold: "The Effect of Interface Roughness and Oxide Film Thickness on the Elastic Response of Thermal Barrier Coatings to Thermal Cycling," *Mater. Sci. Eng.,* 2000, *A284,* pp. 158-75.
10. A.M. Freborg, B.L. Ferguson, W.J. Brindley, and G.J. Petrus: "Modeling Oxidation Induced Stresses in Thermal Barrier Coatings," *Mater. Sci. Eng.,* 1998, *A245,* pp. 182-90.
11. C.H. Hsueh and E.R. Fuller Jr.: "Residual Stresses in Thermal Barrier Coatings: Effect of Interface Asperity Curvature/Height and Oxide Thickness," *Mater. Sci. Eng.,* 2000, *A283,* pp. 46-55.
12. M. Ahrens, R. Vaßen, and D. Stöver: "Stress Distributions in Plasma Sprayed Thermal Barrier Coatings as a Function of Interface Roughness and Oxide Scale Thickness," *Surf. Coat. Technol.,* 2002, *161,* p. 26.
13. S.R. Choi, D.-M. Zhu, and R.A. Miller: "Deformation and Strength Behavior of Plasma-Sprayed ZrO2-8 wt.% Y2O3 Thermal Barrier Coatings in Biaxial Flexure and Trans-Thickness Tension," *Ceram. Eng. Sci. Proc.*, 2000, *21*(4), pp. 653-61.
14. D. Basu, C. Funke, and R.W. Steinbrech: "Effect of Heat Treatment on Elastic Properties of Separated TBCs," *J. Mater. Res.,* 1999, *14*(12), pp. 4643-50.
15. D. Basu, C. Funke, and R.W. Steinbrech: "Instrumentierte Härteprüfung zur Ermittlung des elastischen Verhaltens von plasmagespritzten Wärmedämmschichten" in *Instrumented Hardness Testing for Determination of the Elastic Response of Plasma-Sprayed Thermal Barrier Coatings,* Werkstoffwoche '98, Vol. X, W.J. Muster, J. Ziebs, and R. Linke, ed., Wiley-VCH, 1999, pp. 195-200 (in German).
16. E.F. Rejda, D.F. Socie, and T. Itoh: "Deformation Behavior of Plasma-Sprayed Thick Thermal Barrier Coatings," *Surf. Coat. Technol.,* 1999, *113,* pp. 218-26.
17. H.W. Grünling, K. Schneider, and L. Singheiser: "Some Practical Aspects of Corrosion and Coatings in Utility Gas Turbines," *Mater. Sci. Eng.,* 1987, *88,* pp. 177.
18. G. Blandin, S.E. Brunings, R.W. Steinbrech, and L. Singheiser: "Curvature Behaviour of Multilayer Specimens of Thermal Barrier Systems," *Mater. Sci. Forum,* 2000, *347-49,* pp. 574-79.
19. C-C. Chiu and E.D. Case: "Elastic Modulus Determination of Coating Layers as Applied to Layered Ceramic Composites," *Mater. Sci. Eng.,* 1991, *132,* p. 39.
20. R. Vaßen, M. Ahrens, A.F. Waheed, and D. Stöver: "The Influence of the Microstructure of Thermal Barrier Coating Systems on Sintering and Other Properties," in *Proc. International Thermal Spray Conference 2002* E. Lugscheider and C.C. Berndt, ed., Verlag für Schweißen und verwandte Verfahren DVS-Verlag GmbH, Essen, Germany, 2001, pp. 879-83.
21. W. Weizel: *Lehrbuch der theoretischen Physik—Physik der Vorgänge,* Textbook of Theoretical Physics—Physics of Processes, Vol. 1 Springer Verlag, Berlin, Göttingen, Heidelberg, Germany, 1955.
22. W.N. Findley, J.S. Lai, and K. Onaran: *Creep and Relaxation of Nonlinear Viscoelastic Materials* North-Holland Publishing Company, Amsterdam, The Netherlands 1976, p. 57.
23. W. Kreher and W. Pompe: "Internal Stresses in Heterogeneous Solids" in *Physical Research*, Vol. 9 Akademieverlag, Berlin, Germany 1989.
24. B. Siebert, C. Funke, R. Vaßen, and D. Stöver: "Changes in Porosity and Young's Modulus Due to Sintering of Plasma Sprayed Thermal Barrier Coatings," *J. Mater. Proc. Technol.,* 1999, *92-93,* pp. 217-23.
25. J.A. Thompson and T.W. Clyne: "The Effect of Heat Treatment on the Stiffness of Zirconia Top Coats in Plasma-Sprayed TBCs," *Acta Mater.,* 2001, *49,* pp. 1565-75.
26. R.C. Rossi: "Prediction of the Elastic Moduli of Composites," *J. Am. Ceram. Soc.,* 1968, *51,* pp. 433-40.
27. R.M. Spriggs: "Expression for Effect of Porosity on Elastic Modulus of Polycrystalline Refractory Materials, Particularly Aluminum Oxide," *J. Am. Ceram. Soc.,* 1961, *44,* p. 628.
28. R. Vaßen, N. Czech, W. Malléner, W. Stamm, and D. Stöver: "Influence of Impurity Content and Porosity of Plasma Sprayed Yttria Stabilised Zirconia Layers on the Sintering Behaviour," *Surf. Coat. Technol.,* 2001, *141,* pp. 135-40.
29. M. Kachanov, I. Tsukrov, and B. Shafiro: "Effective Moduli of Solids With Cavities of Various Shapes," *Appl. Mech. Rev.,* 1994, *47,* pp. 151-74.
30. Y. Sakka, Y. Oishi, K. Ando, and S. Morita: "Cation Interdiffusion and Phase Stability in Polycrystalline Tetragonal Ceria-Zirconia-Hafnia Solid Solutions," *J. Am. Ceram. Soc.,* 1991, *74,* pp. 2610-14.